environment as substantiated by the SA-203 orbital liquid hydrogen experiment and depicted in Fig. 1.

References

[1] Majoros, J. and Smith, D. A., "Control of Liquid Entrainment During Venting," *IES Proceedings, 1965*, DAC Technical Paper 3390, McDonnell Douglas Corp.

[2] "Saturn S-IVB-203 Stage Flight Evaluation Report," DAC-SM 46988, March 1967, McDonnell Douglas Astronautics Co., Western Div., Huntington Beach, Calif.

Solid-Propellant Grain-to-Mandrel Adhesion Phenomena

J. D. Burton*

Rocketdyne, A Division of North American Rockwell Corporation, McGregor, Texas

In structural evaluation of propellant grains for solid rocket motors, effects of the cure process are often loosely treated, using strain evaluation cylinder measurements to infer grain response to cure. With the advent of devices for monitoring grain-case bond line stress state during the life cycle of a solid-propellant motor,[1,2] experimental data indicating the influence of cure shrinkage in current standard processes have been generated. Volumetric shrinkage, due in part to polymerization of the binder material during cure, coupled with propellant-to-mandrel adhesion has been detected and gives cause for some concern as to its effect on the grain structural integrity. Observations that define the basic impact of the shrinkage on grain structural integrity and on the analytic evaluation of the integrity are described.

Experimental Observations

The test vehicle for this study was a set of 4-in. analogue motors cast with cylindrical port grains of Carboxyl-terminated polybutadiene(CTPB) propellant with web fractions on the order of 60% and instrumented with through-the-case type normal bond stress transducers, Fig. 1. No liner material was used in these motors. The mandrels used to form the inner port were Teflon†-coated rods after the standard method of motor processing. Tests were also conducted in which the mandrel was covered with tubegauze and the tubegauze covered with a latex membrane. This system, although impractical for real motors, provides a positive mandrel release. Bond line stresses for three motors during propellant cure, typical of the several tests conducted, are shown in Fig. 2. Motor A employed three curative systems to emphasize the effect of polymerization on the grain stress-state during cure. Motors B and C contained the same basic propellant with its standard single curative. Motor B was cast with a

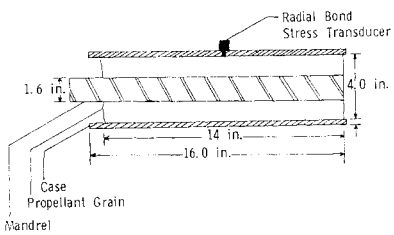

Fig. 1 Instrumented analogue motor.

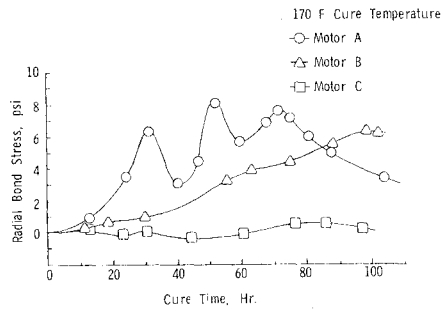

Fig. 2 Cure response.

Teflon-coated mandrel and motor C with the tubegauze-latex system.

Further emphasis on the relation between shrinkage and propellant adhesion to the mandrel is shown in Fig. 3. The response portrayed was measured in the first minutes of cool-down on completion of motor cure. The rapid rise in bond stress is indicative of a highly constrained, nearly incompressible material undergoing shrinkage. As propellant-to-mandrel unbond occurs, the stress is seen to relax in a pattern typical of viscoelastic materials. Motor C, with the positive release system, shows only the response of a cylindrical grain to thermal cool-down and follows the expected stress-time profile. Subsequent reheating of the motors to the cure temperature followed by the same environmental changes gave no spike and further indicated that the phenomena were due to propellant-to-mandrel adhesion.

Summary and Conclusions

In addition to the tests conducted specifically for identification of mandrel adhesion and the cure shrinkage process, observations made on full-scale motors[3] and on numerous strain evaluation cylinders further confirm the results described previously. Concern for the effect of mandrel adhesion stems from the uncertainties introduced by the observed phenomenon. The adhesion is an uncontrolled processing variation that may lead to decreased structural reliability. During the cure period, the propellant is undergoing a change of state and the normal volumetric shrinkage, if prevented by boundary constraints, must lead to the formation of voids or fissures within the grain. Finally, the analysis of the grain structure depends on an assumed stress-free starting point. This starting point is obviously not the end of motor cure and the analysis must, therefore, include the cure period. Insufficient data are available for rigorous analytical treatment of propellant behavior during cure but at least one approach has been proposed to define this behavior.[4]

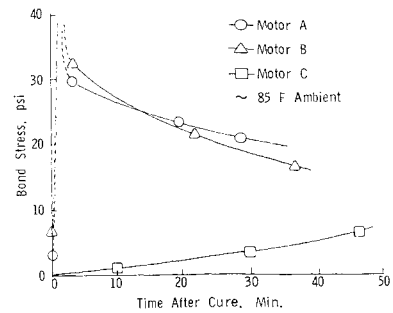

Fig. 3 Spiking phenomena.

References

[1] Burton, J. D., "Solid Propellant Grain-to-Case Bond Stress Measurement," presented at the SESA 1969 Fall Meeting, Houston, Texas, Oct. 1969.

[2] Leeming, H., "The Structural Test Vehicle as an Evaluation Tool for Propellant," AIAA Paper 68-508, Atlantic City, N. J., 1968.

Received October 6, 1969.

* Member of the Technical Staff.

† DuPont trademark for a tetrafluoroethylene plastic.

[3] Miller, W. H., "Experimentally Measured Bond Stresses in a Full-Scale Motor," AIAA Paper 68-510, Atlantic City, N. J., 1968.

[4] Cost, T. L., "Analytical Methods for Determining the Shrinkage Stresses in Polymeric Materials During Cure," TR S-72, Dec. 1968, Rohm and Haas Co., Redstone Research Labs.

High-Fidelity Solar Simulation for an Ultrahigh Vacuum Facility

DEWEY E. WORNOM*
NASA Langley Research Center, Hampton, Va.
AND
F. N. BENNING†
Spectrolab Division of Textron Industries, Sylmar, Calif.

SOLAR simulation has been provided for the Langley Research Center 150-ft[3] Space Vacuum Facility. The facility vacuum chamber, 7½ ft in diameter and 12 ft long, is shown in Fig. 1. The concentric cylindrical walls of the chamber consist of a conventional outer wall, a liquid-nitrogen-cooled inner wall, and an innermost liquid-helium-cooled cryopanel enclosing a 150-ft[3] test volume. The volume within the inner chamber wall is pumped by a main oil diffusion pumping system while a guard volume, between the inner and outer chamber walls, is differentially pumped by a separate oil diffusion pumping system. Access to the test volume is provided by a full-diameter hinged door on the outer wall and removable cylindrical doors on the inner wall and cryopanel. From standard atmospheric conditions, the chamber is capable of obtaining ultimate pressures below 10^{-10} torr within 24 hr. Complete details of the facility and its performance capabilities are given in Refs. 1 and 2.

Chamber Modification for Solar Simulation

The criterion for modifying the chamber for solar simulation was to introduce any additional gas load to the guard volume rather than to the test volume, avoid creating a direct leak from outside the chamber into the test volume, and allow return of the chamber to its original configuration and performance capability when solar simulation was not required. This criterion was satisfied by use of an on-axis type simulator that permitted, as shown in Fig. 2, simple and direct penetration through the chamber doors. Therefore, chamber modification consisted of replacing the chamber doors with new doors having openings approximately 3 ft in diam. Upon coupling the simulator to the outer chamber door, the cylindrical end of the transition cone compresses the metal bellows attached to the inner chamber door opening and the simulator collimating lens becomes the vacuum closure for the opening. And, through ports in the cylindrical end of the cone, the cone volume becomes part of the chamber guard volume with the simulator tipping lens acting as the vacuum closure for the cone. The use of simulator optical elements instead of flat windows as vacuum closures for the door penetrations avoided the unnecessary degradation of the simulator beam that windows would have created.

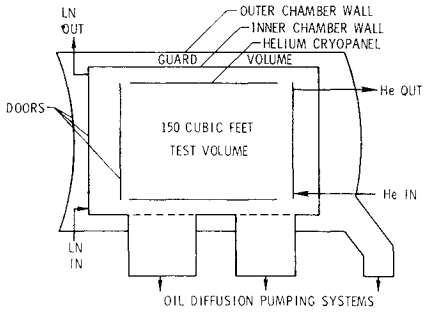

Fig. 1 150-ft[3] space vacuum facility.

Solar Simulator Design

The major components of the simulator system, noted in Fig. 2, consist of thirteen 2.5-kw xenon energy sources, collectors, folding mirrors, field lens assembly, and projection lens assembly, all enclosed within a sealed radiation housing. This housing is continuously purged with cold gaseous nitrogen which acts as a coolant and eliminates formation of ozone. The remaining optical elements, a tipping and a collimating lens, are held within the transition cone that couples the radiation housing to the chamber.

Power for the multiple energy sources is provided by individual power supplies filtered for a d.c. current ripple of less than 1%. System operation is initiated by energizing the energy sources then regulating their current individually or collectively to obtain the selected beam intensity level. Thereafter, the selected intensity is automatically maintained by a light-sensored (sensors located near each source) closed-loop control system. The complete system is operated and monitored from a central control console where annunciation of any cooling or electrical subsystem malfunction is also indicated.

Energy from each source is intercepted then reflected by their collectors onto the first folding mirror. The combined energy of each energy source is then redirected by the folding mirrors into the field lens assembly. This lens assembly, consisting of seven small lenses clustered side by side, separates the circular beam into seven circular light channels. Seven corresponding small lenses in the projection lens assembly intercept and magnify each light channel to fill the collimating lens. Since six of the seven light channels are off of the optical axis, the tipping lens tips these channels to coincide with the collimating lens. The combining of each light channel onto the collimating lens, as well as the energy from each energy source onto the first folding mirror, is for the purpose of improving the uniformity of the beam across its diameter. And, finally, the 36-in.-diam collimating lens provides a 27-in.-diam collimated beam within the chamber test volume.

Also included in the optical system, but not noted in Fig. 2, is a manually operated beam douser that permits beam interruption without de-energizing the energy sources, a beam adjuster that allows adjustment of beam size and shape, and a spectral filter that removes most of the beam spectral content outside of the natural solar spectrum.

Table 1 Solar simulator performance

Simulator characteristics	Test results
Intensity range:	½ to 2 s.c.
Uniformity:	
At ½ s.c.	±6.6%
2 s.c.	±5.6%
Collimation angle:	±3°
Spectral match:	See Table 2
Beam stabilization:	In 12 min
Auto. intensity control:	<1%

Presented as Paper 69-1001 at the AIAA/ASTM/IES 4th Space Simulation Conference, Los Angeles, Calif., September 8–10, 1969; submitted September 29, 1969; revision received November 10, 1969.

* Aerospace Technologist, Applied Materials and Physics Division. Associate Fellow AIAA.

† Technical Director, System Division. Member AIAA.